


Article

Influence of Sea State on Sea Surface Height Oscillation from Doppler Altimeter Measurements in the North Sea

Ferdinando Reale ^{1,*} , Fabio Dentale ^{1,2}, Eugenio Pugliese Carratelli ^{1,2}
and Luciana Fenoglio-Marc ³

¹ Department of Civil Engineering, University of Salerno, 84084 Fisciano, Italy; fdentale@unisa.it (F.D.); epc@unisa.it (E.P.C.)

² Inter-University National Consortium for Marine Sciences (CoNISMa), 00196 Roma, Italy

³ Institute of Geodesy and Geoinformation, University of Bonn, 53115 Bonn, Germany; fenoglio@geod.uni-bonn.de

* Correspondence: freale@unisa.it; Tel.: +39-089-964-112

Received: 31 May 2018; Accepted: 6 July 2018; Published: 10 July 2018



Abstract: This paper reports on an investigation on the influence of waves on the sea surface height error, σ_h , as measured by Delay Doppler satellite altimetry (DDA). CryoSat-2 altimeter sea surface height (SSH) data in the North Sea, processed in both DDA and pseudo low resolution mode (PLRM), are correlated with European Centre for Medium-Range Weather Forecasts (ECMWF) co-located sea state data. We find a small, but consistent correlation between the 1 Hz standard deviation, σ_h , of the 20 Hz altimeter SSH and the ECMWF total significant wave height, SWH_t . The same analysis carried out between σ_h and the swell component of the wave spectrum shows a smaller correlation. In contrast, the correlation between the PLRM σ_h and any component of the SWH spectrum has not been found to be significant. To provide an explanation of these results, the aliasing effect caused by the interaction between the sea wavelength and the altimeter resolution has been considered; a simple model has, therefore, been produced to simulate the dependence of the aliasing-derived, σ_A , on the sea wavelength. The alias/wavelength curve obtained helps to explain why—at least for the relatively low wavelength sea data considered—the wave direction and its wavelength have little or no influence on σ_h .

Keywords: Doppler altimetry; altimeter resolution; sea waves; sea surface height; sea surface height error; aliasing curve

1. Introduction

Delay Doppler mode altimetry (also known as SAR altimetry, in the following DDA or SAR) is designed to achieve higher along-track resolution than classical pulse-limited altimetry (CA, also low resolution mode, LRM); this property can be exploited to increase the number of independent measurements over a given area and it is a prerequisite for sea-ice thickness measurements, coastal waters, ice sheet margins, land, and inland waters [1]. The widening use of DDA onboard satellites, such as CryoSat-2 (C-2) and Sentinel-3 (S-3) [2,3], has raised interest in a new problem, i.e., the compatibility of DDA data with previous CA time series. Significant wave height (SWH) continuity is straightforward, since the requirements for SWH accuracy are relatively minor. Much more relevant is the behavior of the sea surface height (SSH) measurement, i.e., the average—over the extent of many wavelengths—of the instantaneous water height. Continuity between CA and DDA measurements of this latter parameter is vital: All possible sources of errors must, therefore, be carefully considered.

An important effect, known as sea state bias, is the influence of sea waves on the mean SSH as measured by satellite altimetry; this effect, which has been the object of intensive work [4–6], is derived from the skewness of the instantaneous water height and from the difference in Electro-Magnetic (E/M) waves' reflectivity between the crests and the troughs of the sea waves. Another—and perhaps more important—parameter is the SSH noise, i.e., the standard deviation of the SSH measurement (as opposed to the standard deviation of the instantaneous water height, a parameter closely related to SWH). There are many causes of the SSH noise, but one of them is certainly the influence of the sea waves. The main reason for such an effect, according to Dibarboure et al. (2014) [7], is the inhomogeneity in the backscatter strength induced by atmospheric and/or surface factors. The problem may also affect other systems in the future: Peral et al. (2015) [8] carried out a simulated assessment of the impact of waves on error within the frame of the SWOT (Surface Water and Ocean Topography) project.

A useful indicator of such noise is provided by the “SSH error”, i.e., the standard deviation, σ_h , of the 20 Hz SSH. Recently, a connection between σ_h and the longer wavelength components of the sea spectrum has been shown [7,9–12]. A direct comparison between DDA and conventional CA is not trivial, since recent satellites do not perform both measurements at the same time. In CA, pulses are transmitted and received continuously, i.e., they are interleaved, as for all conventional altimeter missions. A low pulse repetition frequency (PRF) of 1800 pulses per second, which is below the Wash limit, is used to ensure that successive pulses are only partially correlated and that noise reduction can be achieved through incoherent averaging. The CryoSat-2 SAR mode is different in that it operates with closed bursts, i.e., the pulses are transmitted and received in bursts of 64 pulses, and the reflected signal reaches the antenna after the end of the transmitted burst. The successive pulses within the bursts are correlated because the PRF is high (18 kHz).

The radar sends a burst of pulses every 11.8 ms and the duration of each burst is 3.5 ms, resulting in no measurement being made 70% of the time [13]. Within each burst, the interval between pulses is 55 μ s [14]. The returning echoes are processed coherently in the along-track direction, thus, synthesizing a 26 m long aperture antenna. This results in a footprint that is beam-limited and narrow in the along-track direction, and pulse-limited and broad (1.5–3 km) in the cross-track direction [2].

The size of the along-track Doppler cell, which gives the along-track resolution, depends on the burst length, the wavelength of the transmitted signal, the velocity, and the height of the spacecraft [2]. These values for CryoSat-2 are 3.5 ms, 2.2 cm, 7498 m/s, and 735 km respectively, with a resulting along-track cell length of 311 m. The pseudo-LRM (PLRM) waveforms generated from CryoSat-2 and Sentinel-3 in the SAR mode are not statistically equivalent to LRM data due to the limited time of transmission and the resulting smaller number of averaged observations.

The accuracy and the precision of DDR have been tested in several studies by comparison with tide gauges, thus, motivating the inclusion of CryoSat-2 sea level measurements in the existing sea level records [15]. The goal of the present analysis is to investigate the influence of sea waves on σ_h , computed with both DDA and PLRM, by correlating the data with sea state indicators obtained in an area where good quality model data are available, as described in the following. We also numerically simulate the aliasing effect, derived from the interaction of sea waves spectral wavelengths with the resolution of the altimeter, to evaluate whether this effect might influence the results.

In Section 2 we describe the methodology and data used. Results are presented in Section 3, discussion is reported in Section 4 and conclusions are discussed in Section 5.

2. Materials and Methods

The study has been carried out on data over the eastern part of the North Sea (Figure 1) during the time interval from July 2010 to May 2014.

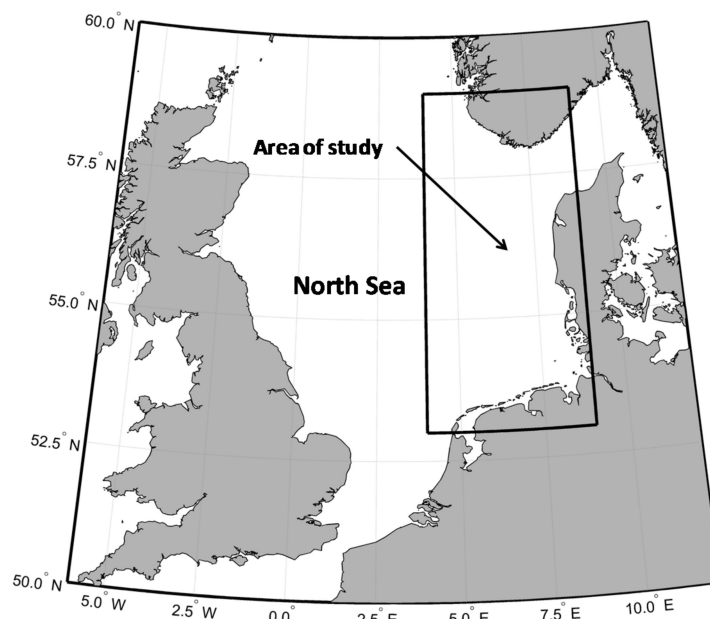


Figure 1. A map of the North Sea. Study area is delimited by the black box and is between 53–59° of latitude and 4–9° of longitude.

CryoSat-2 Level 2 data were extracted from the ESA-ESRIN GPOD platform described in [16]. The corresponding PLRM data were derived from the same full bit rate (FBR) SAR L1A data by using the procedure described in [17]. The computation of σ_h , i.e., of the SSH 20 Hz error defined above, was the same for both PLRM and DDA altimeter datasets. The altimeter data used here, in addition to σ_h , was the 1 Hz SSH and the significant wave height at 1 Hz (SWH).

To provide a reliable set of ground truth sea state data, ECMWF data were obtained from the Meteorological Archival and Retrieval System (MARS), based on the analysis operational archives of the high resolution stand alone wave model (previously limited area model) at 6-h intervals and on a grid with a spatial resolution of $0.125^\circ \times 0.125^\circ$. The data that were considered include the following: Total significant wave height of the whole spectrum, i.e., combined wind waves and swell (in the following SWH_t), significant wave height of wind waves (SWH_w), significant wave height of the swell (SWH_s), their respective average periods (T_t , T_w , T_s), and their directions.

Since ECMWF data were located on a fixed $0.125^\circ \times 0.125^\circ$ grid and at 6-h intervals, which obviously does not coincide with the satellite altimeter track points, the former were co-located over altimeter tracks by using a simple linear interpolation in space and time [18]. For each altimeter, one second measurement, the ECMWF data at time before and after the satellite passage, was individually interpolated over the track point positions (space interpolation); in turn, the two space interpolated values were interpolated over the altimeter time of passage (time interpolation). Each co-located one-second set of model and altimeter values is indicated as an “event” herein.

It is important to fully understand the characteristics of the wave climate considered. Therefore, a statistical analysis was carried out on the data. Table 1 sums up some parameters of the event data set. ASWH is the average SWH computed for all the events over the SWH_t , SWH_w , and SWH_s . SSSWH is the sum of the squares of the SWH of each event, computed separately for the total, wind, and swell components. This parameter was considered because the square of the SWH is proportional to the energy (En) of the wave field, and it is a good indicator of the sea state. Finally $En/Entot$, i.e., the ratio between the energy of each component and the total, is also considered.

Table 1. Repartition of sea state within all ECMWF dataset.

Parameters	SWH _t	SWH _w	SWH _s
ASWH (m)	1.68	1.20	0.94
SSSWH (m ²)	1.54	74,620	37,484
En/Entot	1.00	0.66	0.33

It appears that most of the total wave was given by the wind waves, while swell only accounts of about for one third.

Useful information is also provided by the statistical distributions of the events according to their average wavelength L , corresponding to the average period, T , through Equation (1), which is valid for deep water:

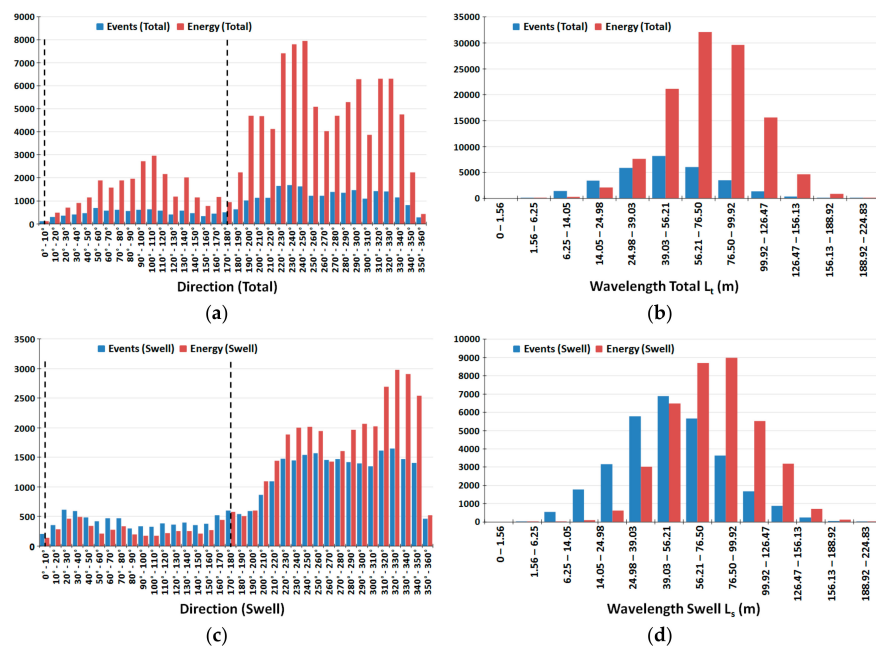
$$L = \frac{gT^2}{2\pi}. \quad (1)$$

The following Table 2 reports the average, and the standard deviation, SD, of the events for the three spectrum average wavelength components (L_t , L_w , and L_s).

Table 2. Average (A) and standard deviation (SD) of the three spectrum average wavelength components for the events in the ECMWF dataset.

Parameters	L_t	L_w	L_s
A (m)	51.92	29.14	73.45
SD (m)	27.83	22.43	38.90

In Figure 2, the distributions of both the number of events and of the square of their SWH (proportional to the energy, therefore, a proxy of the importance of the event) are shown according to their propagation direction and to their wavelength (average wavelength, L_t , for the “Total” data). The flight paths of the satellite are oriented at about 6° and 174° .

**Figure 2.** Distribution of events and event wave energy according to direction (a,c) and wavelength (b,d) for the whole spectrum (a,b) and the swell component (c,d). Dashed lines show the approximate satellite flight direction.

The analysis reported above shows that most of the events have an average wavelength between 40 and 126 m, while most of the energy is located between 25 and 75 m; the situation does not change much if only the swell component is considered (Figure 2d). Very few swell events have a wavelength of more than 156 m. Our data set is, therefore, characterized by generally short wavelengths. Figure 2a,c are also interesting, since they prove that most of the sea state directions are not aligned with the satellite tracks. Both these considerations are useful to understand the results, which will be discussed in the following section.

3. Results

The final objective is to verify whether some of the sea state parameters affect σ_h , and if they affect SAR and PLRM in a different way.

Firstly, we compared the ECMWF wave height, SWH_t , and the altimeter significant wave heights, SWH_{SAR} and SWH_{PLRM} . They were highly correlated, with a correlation of 0.89 for both types of altimeter data (Figure 3). This was expected as satellite measured SWH values are routinely assimilated into ECMWF analysis and re-analysis. Therefore, the quality of the data was excellent and this justifies the choice of the area and of the ECMWF model as a reference.

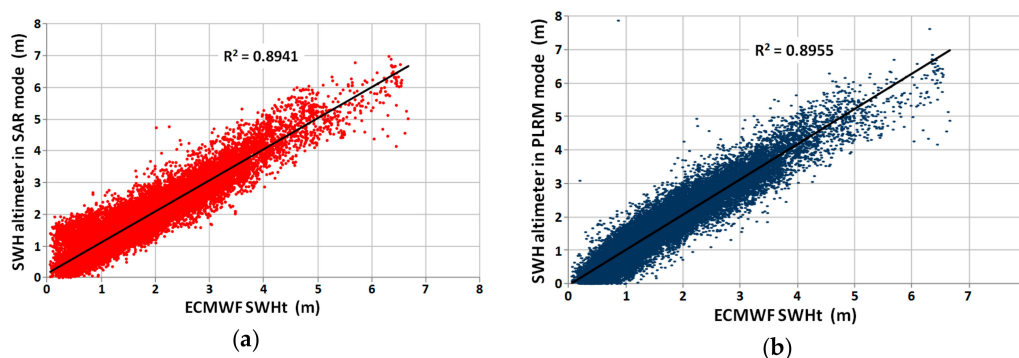


Figure 3. Altimeter versus ECMWF co-located SWH values: (a) Altimeter in SAR mode; and (b) altimeter in PLRM mode.

Furthermore, we investigated a possible correlation between the σ_h of the two altimeter products. Figure 4 shows that the two σ_h are uncorrelated ($R^2 = 0.09$). Moreover, PLRM error was, on average, larger than SAR error: 0.0157 versus 0.0096. This agrees, at least qualitatively, with previous results that have provided a larger PLRM σ_h than SAR σ_h (see, for instance, Figure 1a in [7]).

Finally, we investigated the correlation between the σ_h of both altimeter products and various parameters of the sea states within the data set (see Figure 5 and Table 3).

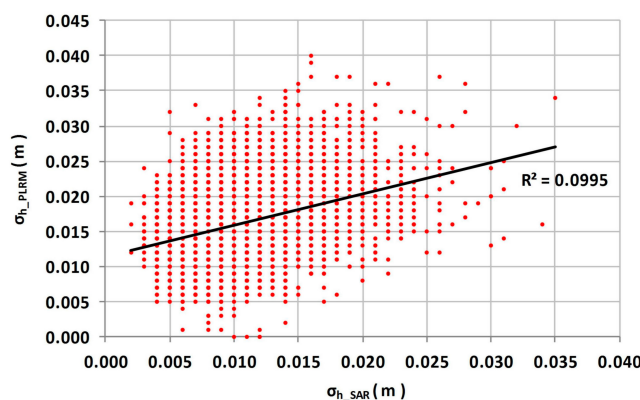


Figure 4. Correlation between the standard deviation, σ_h , of SSH in SAR and PLRM mode.

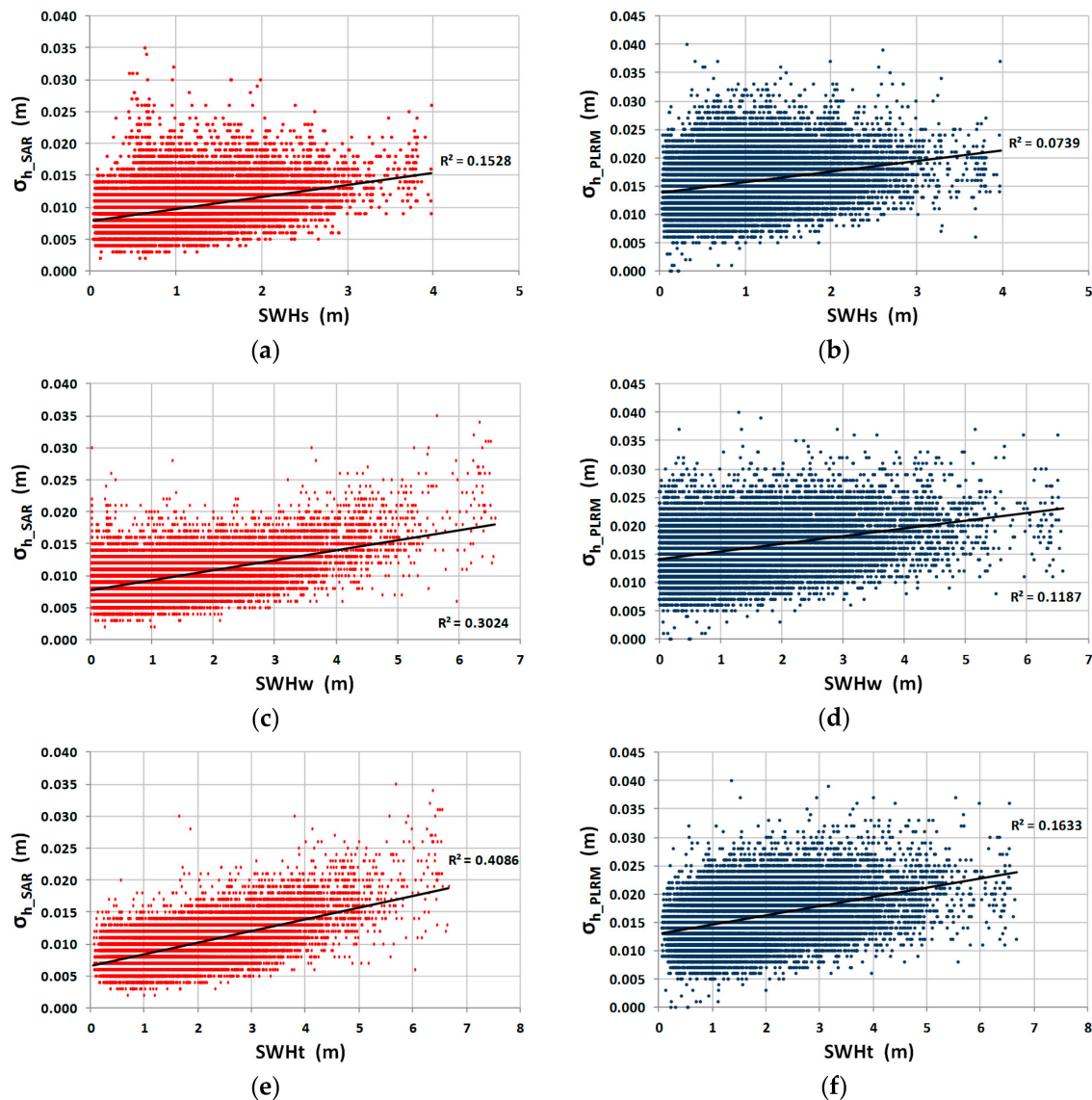


Figure 5. Correlation between the standard deviation, σ_h , of SSH and SWH_s , SWH_w and SWH_t : (a,c,e) altimeter in SAR mode; (b,d,f) altimeter in PLRM mode.

The only relevant result was a modest—but non-negligible—correlation between the total significant wave height, SWH_t , and the SAR 1 Hz standard deviation, σ_h ($R^2 = 0.4$). On the contrary, there was no correlation between either of the two components of the sea spectrum (SWH_s and SWH_w) and SAR or PLRM σ_h (see Table 3).

Table 3. Correlation coefficients, R^2 , between σ_h values for the SAR and PLRM mode and the three SWH components of the wave spectrum.

Altimeter Mode	Swell (SWH_s)	Wind (SWH_w)	Total (SWH_t)
SAR mode	0.15	0.30	0.41
PLRM mode	0.07	0.12	0.11

Similar calculations, carried out on the average periods of the sea state components, show no relevant connection with either SAR or PLRM σ_h values (Table 4).

Table 4. Correlation coefficients, R^2 , between σ_h values for the SAR and PLRM mode and the mean periods of the wave spectrum and of its swell and wind components.

Altimeter Mode	Swell (T_s)	Wind (T_w)	Total (T_t)
SAR mode	0.25	0.26	0.24
PLRM mode	0.11	0.12	0.11

Multiple correlations between σ_h and SWH_t and T_t yield the same results as the respective simple regressions between σ_h and SWH_t , thus, confirming the lack of any simple correlation with the average wave period (Figure 6 and Table 5).

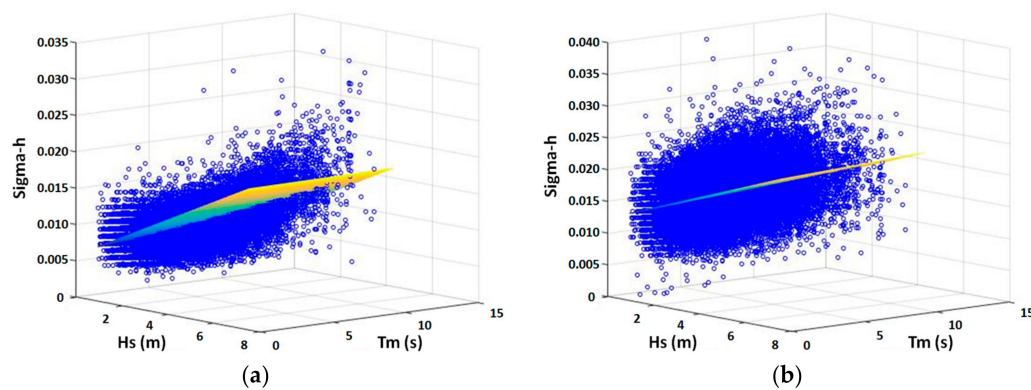


Figure 6. Multiple correlation between σ_h , SWH_t , and T_t both for the SAR (a) and PLRM data (b).

Table 5. Multiple correlation coefficients, R^2 , between σ_h values, SWH_t , and T_t of the total spectrum for the SAR and PLRM data.

Altimeter Mode	Total (SWH_t)
SAR mode	0.41
PLRM mode	0.16

The direction of the wave system should also play a role, however, a simple correlation with the angle, α , between the average wave propagation and the satellite track would not produce any results, since any connection would be strongly non-linear. Therefore, a procedure has been tested to evaluate the influence of α . A threshold, α_{thr} , was applied to the direction of the events considered: Only events where $|\alpha| > \alpha_{thr}$ were considered. See Figure 7.

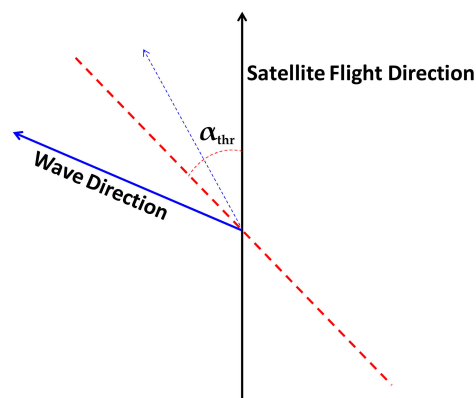


Figure 7. Effect of wave direction: Only events that fall outside the threshold angle α_{thr} are considered.

For instance, if α_{thr} is taken to be 40° , all sea directions whose propagation angle with the flight direction was less than 40° were excluded. The results are shown in Figure 8.

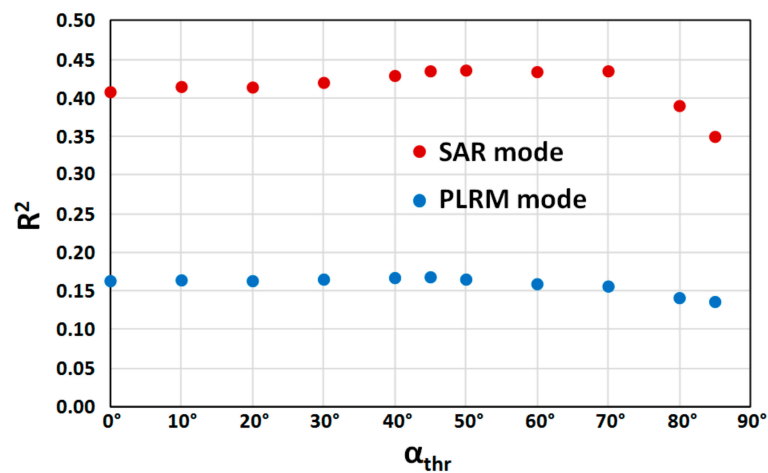


Figure 8. Correlation coefficient between σ_h and SWH_t as a function of the threshold angle, α_{thr} .

Again, the correlation between SWH_t and σ_h was clearly higher for the SAR altimeter data, compared to the same correlation for the PLRM data, this latter being practically negligible ($R^2 = 0.15$), while the former, independently from the threshold, was constantly about 0.40 except for a small decrease as α_{thr} approached 90° : i.e., if only nearly perpendicular events are considered, the correlation decreases.

4. Discussion

We have shown that σ_h , as measured by DDA, had a non-negligible correlation with the total SWH_t , while the correlation was much lower if only the swell component was considered. No such effect exists for the PLRM data considered here.

Furthermore, the relative direction between the wave system and the satellite path seems to bear little or no influence on the SAR σ_h behaviour.

While many physical effects may cause the altimeter SSH noise, the aliasing effect between the SAR altimeter resolution and the sea wavelength should play a role in the formation of σ_h .

A deeper insight can only be gained by numerically investigating the measuring procedure [19,20], thus, a simple conceptual numerical model of the Doppler altimeter (Figure 9) was implemented to evaluate the aliasing effect, which should contribute to the measured σ_h .

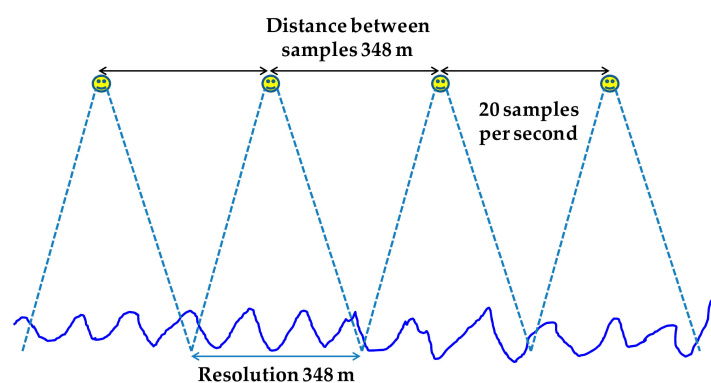


Figure 9. Schematic of the SAR altimeter conceptual model.

A bi-dimensional model was considered, with a fixed angle, α , between the satellite flight path and the wave direction. Spectral numerically simulated JONSWAP (Joint North Sea Wave Observation Project) wave trains, with a significant wave height (H_m), average wavelength period T_m , and corresponding wavelength (L_m), were considered. Indeed, in real life, the waves are far from being sinusoidal: Each sea state is normally made up of a number of components of a spectrum. The surface was sampled at 20 Hz, i.e., 20 samples (looks) over a length of 6960 m. Thus, the distance between samples was 6960/20, which is 348 m, and was comparable to the along-track theoretical resolution of DDA. Therefore, we assume that the along-track altimeter resolution was equal to the sample length at 20 Hz. The error, σ_A , which can be assumed as a proxy of the part of the σ_h induced by the aliasing effect, was computed as the standard deviation of the simulated 20 Hz SSH:

$$\sigma_A = \sqrt{\frac{1}{19} \sum_{i=1}^{20} (h_i - h_m)^2} \quad (2)$$

where h_i is the average SSH over sample i (348 m long) and h_m is the average of h_i over the one second interval (Equation (3)):

$$h_m = \frac{1}{20} \sum_{i=1}^{20} h_i \quad (3)$$

The aliasing effect can then be investigated by varying wave parameters, i.e., H_m and L_m , as well as the angle, α , between the satellite flight path and the wave direction. Figure 10 shows the dependence on α and L_m for a fixed wave height, $H_m = 3$ m.

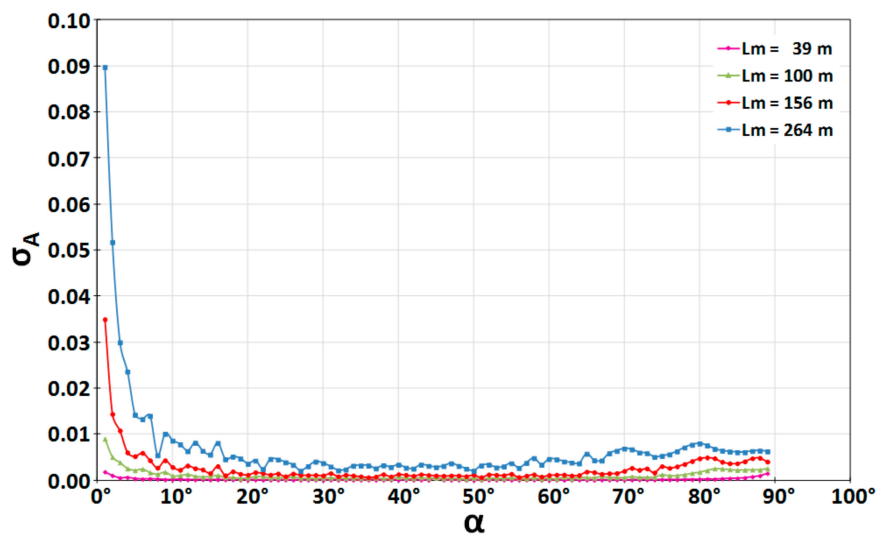


Figure 10. Aliasing effect, σ_A , as a function of the angle, α , between the satellite flight path and the wave direction for four different average wavelengths, L_m , and for a fixed wave height, $H_m = 3$ m.

There are some noteworthy conclusions to make on these results. First, and foremost, the aliasing effect was generally small, except for sea states very closely aligned with the satellite track; for most of the directions, σ_A was of the order of a few millimetres at most (compared with the average $\sigma_h = 1.56$ cm of the experimental DDA values as reported above) and it was basically independent of the angle, α . This result was derived from the use of a realistic spectrum rather than of a single sine wave, so little or no aliasing resonance takes place. It also appears that the length, L_m , did play a role, but even for the highest wavelength considered here ($L_m = 264$ m, $T_m = 13$ s) this was negligible. As it was shown above, very few of the events considered have an average wavelength, L_m , that was over 156 m ($T_m = 10$ s).

It should also be noted that sea states that happen to be strictly aligned with the track would show a relevant σ_A , comparable or even larger than σ_h . This is, however, a rare occurrence that did not appear in the experimental data: As shown above, very few—if any—of the sea states were aligned with the satellite directions.

5. Conclusions

A number of correlations have been carried out on German Bight CryoSat-2 SAR altimeter data to investigate the error of SSH as measured by SAR altimeter, in comparison with conventional simulated low resolution mode PLRM. Results show that, on average, PLRM error is larger than SAR error, confirming previous results and analyses [7].

We also found that the sea state SWH influenced the measurement of SSH for Delay Doppler Altimeter (DDA), introducing a 20 Hz error (σ_h), while it had no influence on PLRM data. DDA σ_h was slightly, but consistently, correlated with the significant wave height, but not to any wavelength parameter.

At least for the case examined, which only covered an area not exposed to the ocean, neither the presence of swell, nor the spectral average periods, were good indicators of SSH oscillation; in other words, wavelength does not seem to affect σ_h .

To verify these results, a bi-directional model of the aliasing curve—simulated alias-induced σ_A versus sea wavelength and direction—was implemented; it was proved that σ_A is generally very small in comparison with the σ_h error except for the direction aligned with the satellite paths. According to these results, the wave climate of the Northern sea—relatively short wind waves, directions that are generally not aligned with the satellite tracks—does not appear to induce any aliasing effect, and this accounts for the lack of correlation of SAR σ_h with the wavelength. It is possible, though, that investigations over open oceans might lead to different results.

Author Contributions: F.D. and L.F.-M. had the original ideas; F.R. carried out most of computations; E.P.C. and L.F.-M. coordinated the work.

Funding: Institutional funding from University of Salerno and University of Bonn.

Acknowledgments: Wave data from Meteorological Archival and Retrieval System (MARS) of ECMWF (European Centre for Medium-Range Weather Forecasts). Altimeter data from the ESA-ESRIN GPOD platform (<https://gpod.eo.esa.int/>). Technical support by ESA, through EO-Project 1172 “Remote Sensing of Wave Transformation” and by C.U.G.R.I. (University Consortium for Research on Major Hazards—University of Naples and Salerno) is gratefully acknowledged.

Conflicts of Interest: The authors declare no conflict of interest.

References

1. Jensen, J.R.; Raney, R.K. Delay/Doppler radar altimeter: Better measurement precision. In Proceedings of the IGARSS '98: Sensing and Managing the Environment: 1998 IEEE International Geoscience and Remote Sensing Symposium, Seattle, WA, USA, 6–10 July 1998; Stein, T., Ed.; Institute of Electrical and Electronics Engineers, Inc.: Piscataway, NJ, USA, 1998.
2. Raney, R.K. The Delay/Doppler Radar Altimeter. *IEEE Trans. Geosci. Remote Sens.* **1998**, *36*, 1578–1588. [[CrossRef](#)]
3. Wingham, D.J.; Wallis, D.W. The Rough Surface Impulse Response of a Pulse-Limited Altimeter with an Elliptical Antenna Pattern. *IEEE Antennas Wirel. Propag. Lett.* **2010**, *9*, 232–235. [[CrossRef](#)]
4. Benassai, G.; Migliaccio, M.; Montuori, A. Sea wave numerical simulations with COSMO-SkyMed© SAR data. *J. Coast. Res.* **2013**, *1*, 660–665. [[CrossRef](#)]
5. Reale, F.; Dentale, F.; Carratelli, E.P. Numerical Simulation of Whitecaps and Foam Effects on Satellite Altimeter Response. *Remote Sens.* **2014**, *6*, 3681–3692. [[CrossRef](#)]
6. Xu, Z.; Zhou, W.; Sun, Z.; Yang, Y.; Lin, J.; Wang, G.; Cao, W.; Yang, Q. Estimating the Augmented Reflectance Ratio of the Ocean Surface When Whitecaps Appear. *Remote Sens.* **2015**, *7*, 13606–13625. [[CrossRef](#)]
7. Dibarboure, G.; Boy, F.; Desjonqueres, J.D.; Labroue, S.; Lasne, Y.; Picot, N.; Poisson, J.C.; Thibaut, P. Investigating Short-Wavelength Correlated Errors on Low-Resolution Mode Altimetry. *J. Atmos. Ocean. Technol.* **2014**, *31*, 1337–1362. [[CrossRef](#)]

8. Peral, E.; Rodríguez, E.; Esteban-Fernández, D. Impact of Surface Waves on SWOT's Projected Ocean Accuracy. *Remote Sens.* **2015**, *7*, 14509–14529. [CrossRef]
9. Hwang, P.A.; Plant, W.J. An analysis of the effects of swell and surface roughness spectra on microwave backscatter from the ocean. *J. Geophys. Res.* **2010**, *115*. [CrossRef]
10. Gommenginger, C.; Cipollini, P.; Snaith, H.; West, L.; Passaro, M. SAR altimetry over the open and coastal ocean: Status and Open issues. In Proceedings of the Ocean SAR Altimetry Expert Group Meeting, Southampton, UK, 26–27 June 2013; Available online: http://www.satoc.eu/projects/CP4O/docs/SARALT_EG_pdfs/cg1_CP4O_SARExpert_2627June2013.pdf (accessed on 15 February 2018).
11. Gommenginger, C.; Martin-Puig, C.; Amarouche, L.; Raney, R.K. *Review of State of Knowledge for SAR Altimetry over Ocean. Report of the EUMETSAT JASON-CS SAR Mode Error Budget Study*; EUMETSAT Reference, EUM/RSP/REP/14/749304, Version 2.2; National Oceanography Centre: Southampton, UK, 2013; p. 57.
12. Moreau, T.; Labroue, S.; Thibaut, P.; Amarouche, L.; Boy, F.; Picot, N. Sensitivity of SAR Mode Altimeter to Swell Effect. In Proceedings of the CryoSat Third User Workshop, Dresden, Germany, 12–14 March 2013; Ouwehand, L., Ed.; ESA Communications ESTEC: Noordwijk, The Netherlands, 2014.
13. Garcia, E.S.; Sandwell, D.T.; Smith, W.H.F. Retracking CryoSat-2, Envisat and Jason-1 radar altimetry waveforms for improved gravity field recovery. *Geophys. J. Int.* **2014**, *196*, 1402–1422. [CrossRef]
14. Galin, N.; Wingham, D.J.; Cullen, R.; Fornari, M.; Smith, W.H.F.; Abdalla, S. Calibration of the CryoSat-2 Interferometer and Measurement of Across-Track Ocean Slope. *IEEE Trans. Geosci. Remote Sens.* **2013**, *51*, 57–72. [CrossRef]
15. Fenoglio-Marc, L.; Dinardo, S.; Scharroo, R.; Roland, A.; Dutour Sikiric, M.; Lucas, B.; Becker, M.; Benveniste, J.; Weiss, R. The German Bight: A validation of CryoSat-2 altimeter data in SAR mode. *Adv. Space Res.* **2015**, *55*, 2641–2656. [CrossRef]
16. Dinardo, S.; Fenoglio-Marc, L.; Buchhaupt, C.; Becker, M.; Scharroo, R.; Fernandes, M.J.; Benveniste, J. Coastal SAR and PLRM altimetry in German Bight and West Baltic Sea. *Adv. Space Res.* **2017**. [CrossRef]
17. Buchhaupt, C.; Fenoglio-Marc, L.; Dinardo, S.; Scharroo, R.; Becker, M. A fast convolution based waveform model for conventional and unfocused SAR altimetry. *Adv. Space Res.* **2017**. [CrossRef]
18. Reale, F.; Dentale, F.; Carratelli, E.P.; Torrisi, L. Remote Sensing of Small-Scale Storm Variations in Coastal Seas. *J. Coast. Res.* **2014**, *30*, 130–141. [CrossRef]
19. Carratelli, E.P.; Dentale, F.; Reale, F. Numerical Pseudo-Random Simulation of SAR Sea and Wind Response. In Proceedings of the Advances in SAR Oceanography from Envisat and ERS Missions (SEASAR 2006), Frascati, Italy, 23–26 January 2006; Lacoste, H., Ouwehand, L., Eds.; ESA Publications Division ESTEC: Noordwijk, The Netherlands, 2006.
20. Montuori, A.; Ricchi, A.; Benassai, G.; Migliaccio, M. Sea Wave Numerical Simulations and Verification in Tyrrhenian Coastal Area with X-Band Cosmo-SkyMed SAR Data. In Proceedings of the ESA, SOLAS & EGU Joint Conference “Earth Observation for Ocean-Atmosphere Interactions Science”, Frascati, Italy, 29 November–2 December 2011; Ouwehand, L., Ed.; ESA Communications ESTEC: Noordwijk, The Netherlands, 2012.



© 2018 by the authors. Licensee MDPI, Basel, Switzerland. This article is an open access article distributed under the terms and conditions of the Creative Commons Attribution (CC BY) license (<http://creativecommons.org/licenses/by/4.0/>).